Master clock-thalamic-prefrontal circuit controls circadian social priority

Jihoon Kim[1,2], Jinsun Yu[1,3], Boil Kim[1], Minseok Kim[1,2], Inah Park[1,2], Cheol Song[4], Yulong Li[5], Kyungjin Kim[1], Jong-Cheol Rah[1,3], Han Kyoung Choe[1,2]

[1]Department of Brain Sciences, Daegu Gyeongbuk Institute of Science and Technology; Daegu, 42988, Republic of Korea
[2]Convergence Research Advanced Centre for Olfaction, Daegu Gyeongbuk Institute of Science and Technology; Daegu; Daegu, 42988, Republic of Korea
[3]Korea Brain Research Institute; Daegu, 41062, Republic of Korea
[4]Department of Robotics and Mechatronics Engineering, Daegu Gyeongbuk Institute of Science and Technology; Daegu, 42988, Republic of Korea
[5]National Biomedical Imaging Center, Peking University; Beijing, 100871, China

*Corresponding author. Email: choehank@dgist.ac.kr

Abstract: Social behaviors arise from complex brain operations that adapt to intricate targets and varying states. Achieving a singular social goal requires an extensive social brain network, of which computation is malleable and subject to modulation by diverse internal factors. However, how the brain leverages its internal state to navigate competing social goals is elusive. Here we show that the priority between competing instincts—social novelty versus sexual preference—exhibits a distinct circadian pattern. This is controlled by a two-component circuit linking the master clock in the suprachiasmatic nucleus (SCN) to the medial prefrontal cortex (mPFC), a key brain region in the social brain network. Specifically, SCN^{VIP} neurons project to Vipr2-expressing neurons within the thalamic nucleus reuniens (RE), which in turn projects to the mPFC to mediate this behavior. The function of Vipr2 in the RE is critical for shaping the circadian pattern of both appetitive and consummatory social behaviors. This allows higher social functions to be engaged in a timely manner, appropriately aligning prioritized social behaviors with the body's clock-regulated reproductive system. Overall, this SCN-RE-mPFC circuit provides a neural principle through which the master clock coordinates the prefrontal cortex to resolve a conflict of motivated behaviors by referencing an internal state.

Social behavior is comprised of a diverse repertoire of behaviors, such as mating, attacking, nurturing, or investigating, each of which serves distinct purposes (*1–3*) . In complex social situations, there is a need for robust action prioritization due to the simultaneous exposure of multiple social cues representing different motivations. This intricate nature of social contexts necessitates a mechanism that can evaluate and prioritize competing behavioral options (*4–6*). While the circuitry underlying many innate social behaviors has been extensively studied, the neural mechanism responsible for such behavioral prioritization between different behavioral expressions remains elusive.

One potential target that may function as a social prioritization mechanism is circadian rhythm. Circadian rhythm plays a crucial role in regulating daily homeostasis and maintaining biological rhythms (*7*). Numerous biological processes both from bodily organs and brain functions exhibit 24-hour rhythm, which is governed by the suprachiasmatic nucleus (SCN), a hypothalamic region known as the master clock (*8*). Neurons in SCN maintain synchronized molecular clockworks, enabling self-sustaining circadian rhythm that is independent of external light signals and ensure the synchronized circadian rhythm throughout the brain via the neural or humoral pathways (*9–11*) . Recent studies demonstrated that many behaviors display circadian rhythmicity, which are driven by the SCN (*12–16*). The rhythmic signals originating from the SCN can induce certain behaviors to be prominently expressed at a specific time, resulting in a diverse range of behavioral outcomes depending on the time. While there have been studies on social behaviors that display circadian rhythm, it remains to be demonstrated whether circadian rhythm can prioritize social behaviors in a time-dependent manner.

In order to investigate the influence of circadian rhythm on social behaviors, we developed a behavioral paradigm to assess behavioral prioritization between two distinct social cues. In this paradigm, mice were presented simultaneously with two innately attractive cues: a novel social target and a potential mating partner. We observed significant differences in the investigation patterns exhibited by mice during the early active phase (CT12) compared to the mid-active phase (CT18), indicating circadian modulation of social prioritization. We manipulated genetically labeled SCN neural populations and their projections, identifying SCN vasoactive intestinal peptide (VIP)-expressing neuronal projection to the nucleus reuniens (RE), and RE VIP receptor 2 (VIPR2) neural projection to medial prefrontal cortex (mPFC) mediate circadian shaping of social prioritization. Further examination of RE region revealed tonic increase of VIP in the mid-active phase, suggesting a crucial role of VIP-VIPR2 signaling in RE in shaping the prioritization of social behaviors in a time-dependent manner.

Results

Circadian rhythm in social priority

To evaluate the priority between competing social goals, we developed the social priority test. The test drives behavioral choice by establishing an approach-approach conflict between two instincts: the drive for sexual preference and social novelty (*17*, *18*) . The protocol unfolds in two stages, a familiarization session and a subsequent prioritization session (Fig. 1A). In the familiarization session, we placed a male subject mouse in a 3-chambered arena, presenting a novel female and a non-social object in separate chambers. In the prioritization session, a familiarized female and a novel male were presented in a non-biased counterbalanced manner. We performed the social priority test at four time points throughout the day (CT00, 06, 12, 18). During the familiarization session, male subject mice consistently spent more time exploring the

female cage (fig. S1, A and B). In the prioritization session, they explored both the familiar female cage and the novel male cage; however, this tendency varied depending on the circadian time (Fig. 1, B and C). At CT12, the onset of the active phase, stronger social novelty seeking was observed, while sexual preference was more prominent at CT18, the middle of the active phase. The total moved distance and total interaction time did not differ across all time points (Fig. 1, D and E, and fig. S1, C and D).

We then investigated whether the singular social instincts that constitute our approach-approach conflict exhibit their own circadian rhythms. We found that sexual preference remained constant regardless of the time of day, with no changes in control metrics such as total interaction time or distance moved (fig. S1, E to H). Similarly, the drive for social novelty, as measured by the social recognition test, also showed no circadian rhythmicity (fig. S1, I and J). Again, interaction time and moved distance in this test were consistent across all tested time points (fig. S1, K and L). We also investigated whether female mice also exhibit a circadian rhythm of social priority. When females served as the subjects, the social priority test revealed no significant differences in either familiarization or prioritization session of social priority, total interaction time, or distance moved across the day (fig. S2, A to D). These results were independent of the subject female's estrus cycle. Likewise, in female subjects, neither the sexual preference test nor the social recognition test revealed circadian patterns for the investigation index, total interaction time, or moved distance (fig. S2, H to O).

A following question was whether the rhythm of social priority originates from the internal time of the subject or the target animal. To disentangle these factors, we designed a misalignment experiment focusing on two pivotal time points, CT12 and CT18, where priority shifts from zero (fig. S3, A and B). We created four experimental groups by mismatching the circadian times of subjects and targets from these two time points. During the familiarization session, all four groups behaved comparably, showing no differences in investigation index or total interaction time, with only minor variations in distance moved (fig. S3, C to E). Importantly, a significant difference emerged during the prioritization session. Groups with subjects at CT12 exhibited a novelty-seeking bias regardless of the target's circadian time, whereas groups with subjects at CT18 showed a consistent sexual preference bias (fig. 3F). Across these combinations, there was no difference in total interaction time, and while there was a statistically significant difference in distance moved, the magnitude was marginal (fig. S3, G and H).

Master clock to thalamic circuit for the circadian transition of social priority

Then, we asked how circadian clock shapes the daily pattern of social priority. Mammalian master clock resides in the SCN to convey circadian information to other brain regions and organs through neural and humoral pathway (*8*) . The SCN consists of two major neural populations: VIP(+) and AVP(+) neurons (*19*) . We investigated either the activity of SCN^{VIP} or SCN^{AVP} neurons is required for the circadian control of social priority. We injected AAV-DIO-eNpHR3.0 into the SCN of either VIP-IRES-Cre or AVP-IRES-Cre mice and implanted optical fibers above the SCN (Fig. 1, F and G, and fig. S4, A and B). After incubation and entrainment, the social priority tests were performed with optogenetic inhibition (Fig. 1H). During the initial phase of the social priority test, the familiarization session, the optogenetic inhibition did not affect the investigation toward female, total interaction, or moved distance (fig. S4, C to E). The inhibition of SCN^{VIP} neurons inhibited the prioritization of sexual preference at CT18, while the inhibition of SCN^{AVP} neurons did not alter the transition of social priority between CT12 and CT18 (Fig. 1, I to K). The distance moved and the total amount of social interaction during the

prioritization session was not affected by optogenetic inhibition (Fig. 1, L and M). The results show that SCN^{VIP} neurons shapes the circadian pattern of social priority.

To investigate the neural mechanism by which SCN^{VIP} neurons regulate the circadian pattern of social priority, we first performed anterograde tracing by injecting AAV-DIO-EGFP into the SCN of VIP-IRES-Cre mice (fig. S5). Similar to previously studies, we observed EGFP-positive neural projections in several brain regions, such as the paraventricular nucleus of the hypothalamus (PVH), the RE, the paraventricular nucleus of the thalamus (PVT), and the medial preoptic area (MPOA) – forming predominantly vertical projections (fig. S5).

We then performed optogenetic inhibition of SCN^{VIP} neuronal terminals within each of these regions. The optical fiber was implanted above one of the SCN^{VIP} target regions in SCN^{VIP}-specific eNpHR3.0-expressing mice (Fig. 1, N and O; fig. S5). Then we tested the social priority with optogenetic inhibition of the SCN^{VIP} neuronal terminals (Fig. 1P). None of optogenetic inhibition affect the investigation index, total interaction time, or moved distance during the familiarization session (fig. S5). While the inhibition of SCN^{VIP} projection targeting MPOA, PVT, or PVH did not affect the pattern of social priority at CT12 and 18, the inhibition of SCN^{VIP}-RE projection blocked the priority of sexual preference at CT18 (Fig. 1, Q and R). The index showing the transition between CT12 and 18 also indicated the lack of priority transition in SCN^{VIP}-RE-inhibited animals (Fig. 1S). In all groups, the distance moved during the prioritization session remain unaffected (Fig. 1, T and U).

VIPR2 signaling in the RE

Next, we asked VIP peptide signaling mediates the circadian pattern of social priority and, if so, through which receptor. VIP, a 28 amino-acid-long peptide, acts upon two different types of receptors, VIPR1 and VIPR2 (*20*) . Using intracerebroventricular injection, we pharmacologically blocked pan-VIPR, VIPR1, and VIPR2, respectively, and investigated the transition in social priority (Fig. 2, A to C, and fig. S6A) (*21*, *22*) . The inhibition of both VIPRs blunted the prioritization of sexual preference at CT18, which was recapitulated by VIPR2 antagonist infusion (Fig. 2, D and E). The pharmacological inhibition of VIPR1 did not show behavioral effects. This pattern is obvious in transition index (Fig. 2F). While total total amount of interaction time was comparable to vehicle-injected group, the moved distance during the prioritization session was affected by the infusion of VIPR antagonists (Fig. 2, G and H). Though female investigation of animals infused with pan-VIPR antagonist at CT12 was statistically higher, most behaviors during the familiarization session were comparable to the vehicle-injected group (fig. S6, B to D).

To visualize the Vipr2-expressing cells within the terminal field of the SCN^{VIP}-RE circuit, we crossed Vipr2-IRES-Cre mice with Ai14 reporter mice. This revealed tdTomato reporter expression in the RE (Extended Fig. 7a-c), specifically within the same subregion targeted by SCN^{VIP} neuron projections (fig. S7, A and D). We then examined the function of Vipr2 in the RE by conditionally knocking out Vipr2 in the RE (Fig. 2, I to K; fig. S7, E and F). In contrast to EGFP-expressed control group, the investigation index at CT18 of RE-specific Vipr2 KO significantly biased toward novel male investigation (Fig. 2, L and M), leading to the lack of normal transition between CT12 and 18 (Fig. 2N). There was no difference in moved distance and total interaction time between EGFP- and Cre-expressing groups (Fig. 2, O and P) as well as behavioral measures during the familiarization session (fig. S7, G to I).

Behavioral effects of pharmacological and genetic manipulation of Vipr2 demonstrated main effects in CT 12 and CT18. This raised questions regarding how VIP concentrations change in

the RE region in these time points. We adopted GPCR-based VIP sensor ($GRAB^{VIP}$) in the RE of Vipr2-IRES-Cre KI mice and recorded the $GRAB^{VIP}$ intensity in CT12 and CT18 (Fig. 3, A to C) (*23*) . $GRAB^{VIP}$ intensity in the RE was higher in CT18 than CT12 (Fig. 4, D and E), indicating increased RE VIPergic tone at CT18. We then asked whether the tonal increase of VIP in RE region can differentially regulate neural activity of RE^{Vipr2} neurons in response to social cues. To confirm this, we recorded bulk calcium activity of RE^{Vipr2} neurons during social priority assay between CT12 and CT18, and compared social cue-induced calcium transient (fig. S8, A and B). Calcium transient, aligned to the onset of the investigation of either novel male or familiar female target, showed no change upon cue investigation (fig. S8C). There was also no difference in calcium activity between CT12 and CT18. Combined with $GRAB^{VIP}$ recording, these results suggest that activity of RE^{Vipr2} neurons does not directly encode social cue responsiveness.

Next, we investigated electrophysiological effect of VIPR2 activation in RE^{Vipr2} neurons by whole-cell patch clamp (Fig. 4F). VIP peptide puffs were delivered near fluorescently labeled RE^{Vipr2} neurons through AAV-DIO-EGFP expression (Fig. 4G). This resulted in the robust VIP peptide puff-induced currents (Fig. 4H). In responsive neurons, a 2-second puff produced an almost immediate inward current, with no additional current generated upon washout in most cases. The VIPR agonist significantly depolarized in RE^{Vipr2} neurons, especially in neurons with a low resting membrane potential (Fig. 4, I and J). To summarize, the VIPergic tone in the RE region increases at CT18, and elevated VIP signaling electrophysiologically activates RE^{Vipr2} neurons.

Thalamo-cortical circuit for social priority

With neural connections with various brain areas including mPFC or hippocampus, RE has been implicated in various behaviors in social aspect as well as flexible behavioral control, positioning itself as a candidate for regulating social priority (*24*) . To determine the causal role of RE^{Vipr2} neurons in prioritizing between social novelty and sexual preference, we bidirectinally manipulated their activity at CT12 and CT18 by optogenetics (Fig. 4, A to C; fig. S9, A and B). Optogenetic inhibition through eNpHR consistently biased the mice toward investigating the novel male at both time points (Fig. 4, D and E). Conversely, optogenetic activation via ChR2 biased them toward the familiar female, promoting sexual preference. Crucially, both manipulations abolished the normal circadian transition of social priority (Fig. 4F). These effects were specific, as they did not alter the total interaction time or the total distance moved (Fig. 4G and H), and had minor effects on behavioral measures during the familiarization session (fig. S9, C to E).

To further understand the role of the RE in social prioritization, we explored the downstream target of RE^{Vipr2} neurons. RE reportedly project to the mPFA, hippocampus, and ZI (*25*) . To trace downstream target of RE^{Vipr2} neurons, we expressed EGFP in Vipr2 neurons in the RE (fig. S10, A and B). RE^{Vipr2} neurons almost exclusively project to the mPFC, but not to either the hippocampus or ZI. We then optogenetically inhibited this neural circuit during the social priority test (Fig. 4, I to K; fig. S10, C and D). The inhibition of RE^{Vipr2}-mPFC terminal blocked the investigation of familiar female at CT18 (Fig. 4, L and M). The RE^{Vipr2} neural circuit connecting to the mPFC mediates the transition of social priority between CT12 and 18 (Fig. 4N), without affecting the total interaction time or the total moved distance (Fig. 4, O and P) as well as behavioral measures in the familiarization session (fig S10, E to G). Together, these results indicate that neural projection from RE^{Vipr2} neurons to mPFC shapes circadian rhythm in social priority.

Circadian social priority in naturalistic triadic dynamics

Next, we asked whether the neural mechanisms described so far drives social behaviors of a freely behaving triad. We developed another behavioral test, called TMI (three mice interaction) assay (Fig. 5B), where the subject and two target mice were allowed to interact in an open arena. The scheme of TMI is similar to that of social priority assay. We first introduced a novel female mouse to a subject male mouse for familiarization. After 2 min, another male mouse, novel to both subject male and the female, was placed into the arena. This allowed us to observe the behavior between the subject male and the familiar female and also between the subject male and novel male. We record the behaviors of the three mice and analyzed social and sexual behavior of the subject mice.

To address the function of Vipr2, we specifically knockouted Vipr2 in the RE by injecting AAV-Cre in the RE of Vipr2fl/fl (RE-Vipr2KO) (Fig. 5A). We performed the TMI assay at CT12 and CT18, respectively. The appetitive approach toward the familiar female and the novel male quantitatively differs dependent upon time of a day. The investigation index of EGFP-injected control showed enriched investigation toward the novel male (social novelty prioritized) at CT12 and toward the familiar female (sexual preference prioritized) at CT18 (Fig. 5C). This temporal pattern of the social priority is in accordance with the results of the social priority test. The investigation of RE-Vipr2KO consistently biased toward the novel male at both CT12 and 18 (Fig. 5C). There were no temporal patterns in neither total interaction time nor total moved distance in both genotypes (Fig. 5, D and E). As an internal control, we also compared social priority of target male mice during TMI assay (fig. S11A). Unlike the subject mice, target male mice were exposed to both mice simultaneously, removing the difference in social novelty. In this case, target male mice showed no change in social priority between CT12 and CT18, suggesting the interplay between sexual and social novelty preference in different circadian time (fig. S11, B to D). Taken together, these results suggest that the Vipr2 expression in RE is required for the circadian transition of social priority in a freely behaving triad.

Finally, we explored how the circadian rhythm in social priority during the appetitive phase influences the consummatory action of social behavior, specifically reproductive behavior. We continuously recorded direct social interactions among three mice following a TMI assay. In control animals, a subset of subject males attempted to mount the female (Fig. 5F). Notably, mounting attempts were observed in a greater number of control mice and occurred more frequently at CT18 than at CT12. The latency to mounting was also significantly shorter at CT18 compared to CT12 (Fig. 5G). This suggests that the time point where sexual preference seeking is prioritized coincides with more active sexual behavior. However, RE-Vipr2KO mice rarely attempted mounting at both CT12 and CT18 (Fig. 5, F and G). Interestingly, they permitted intruder target mice to attempt mounting (fig. S11, E and F). While the cumulative rate showed a rapid increase in mounting in control CT12 compared to control CT18, RE-Vipr2KO mice did not achieve successful mounting attempts (Fig5H; fig. S11G). Together, the data indicates Vipr2 function in the RE regulates the circadian patterns of both appetitive and consummatory phase of social behaviors.

Discussion

Social behavior is dynamically shaped by internal states and the identity of interacting partners, yet the neural circuit mechanisms governing these complex decisions are poorly understood. A significant limitation in the field is that research has predominantly employed tasks with single social goals, hindering a comprehensive framework for how the brain translates the control of

simple behaviors into the richness of real-world social interactions. Here, we address this reductionist gap by investigating social priority where three animals engage. Our work reveals a top-down regulatory mechanism in higher brain centers, evidenced by the fact that animals' choices transited between the first and the second half of the active phase, while their fundamental capacities for social recognition and sexual approach remained constant. This circadian prioritization was further confirmed in our freely moving triad TMI assay, which similarly demonstrated that preferences for social novelty and sexual interaction were time-of-day dependent. Critically, we pinpoint that the transition in priority across these two independent assays is driven by VIP-VIPR2 signaling in the RE. Therefore, we propose that the interplay between the master clock-thalamocortical pathway and local VIP-VIPR2 signaling is a key neural principle governing the circadian orchestration of social priorities.

What is the function of circadian social priority between social novelty preference and sexual preference? Circadian rhythmicity is prominent within the reproductive system, where events such as the surge in the hormonal levels of hypothalamus-pituitary-gonad (HPG) axis and ovulation exhibit distinct circadian patterns (*26*, *27*). This circadian pattern produces a temporal window with superior reproductive efficiency (*13*, *28*) . Considering the long refractory period in mice, the importance of aligning reproductive behavior with reproductive physiology via circadian regulation is readily apparent. The circadian regulation of social behavior is particularly pronounced during the consummatory phase, with the clear circadian patterns of reproductive and aggressive behaviors serving as prime examples. The circadian pattern of social priority can provide a temporal filter to match the types of social behavior from appetitive to consummatory phase. Paradoxically, however, sexual preference assays for a single enclosed partner in a three-chamber arena do not show a discernible circadian pattern. The fact that we could detect this pattern using our social priority test with two enclosed partners raises a cautionary note about the use of overly reductionist models in understanding the mechanisms of social regulation.

Circadian rhythms profoundly impact physiological functions, motivation, emotion and higher brain functions (*7*, *29*, *30*) . However, a significant gap in our knowledge persists: while the circadian control of physiology, motivation, and emotion has been extensively characterized, the mechanisms governing higher-order cognition remain elusive. Our study discovers a functional novel circuit where VIP neurons of the master clock (SCN) communicate with the mPFC through the RE. This represents the first demonstration of a neural circuit through which the SCN can exert temporally precise excitatory influence over the prefrontal cortex. We propose that this pathway provides a sophisticated mechanism for fine-tuning cognitive processes. Specifically, the dynamic changes in RE VIPergic tone during the active phase can orchestrate the nuanced, time-of-day-dependent modulation of higher brain functions.

In the present study, by incorporating the circuit connection to the master clock, SCN, we were able to elucidate the role of RE in coordinating instinctive social behaviors. These findings highlight the importance of circadian rhythm on controlling how social instincts are temporally organized in daily life and calls for further examinations of how circadian rhythm impacts various instinctive behaviors.

Materials and Methods

Animals

All procedures were approved by the Institutional Animal Care and Use Committee of the Daegu Gyeongbuk Institute of Science and Technology (DGIST). Adult male C57BL6/J, *Vip-ires-Cre* (#010908, Jackson Laboratory), *Avp-ires-Cre* (#023530, Jackson Laboratory), *Vipr2-floxed* (#035395, Jackson Laboratory), *Vipr2-ires-Cre* (#031332, Jackson Laboratory), and Ai14 (#007914, Jackson Laboratory) mice were reared in standard cages (16□×□36□×□12.5 cm3) and housed under 12-h light/dark cycle (light on from 01:00 to 13:00) with water and food available ad libitum. Mice were weaned from same-sex littermates at approximately 3-4 weeks of age. Mice of age 8–10 weeks were used in the experiments. All behavioral experiments were performed under dimly lit red light conditions.

AAV Production

Adeno-associated virus (AAV) vector expressing $GRAB^{VIP1.0}$ was packaged as previously described, with modifications (*31*). After the production of AAV, their genomic copies were quantified using real-time qPCR. The AAVs were diluted in PBS to a final concentration of 8.12 X 10^{12} genomic copies per milliliter (GC/mL) before the experiments.

AAV and Stereotaxic Surgery

AAV used for the experiments are as follows: AAV1-Ef1a-DIO-eNpHR3.0-EYFP (GC/mL; Addgene), AAV1-Ef1a-DIO-ChR2-EYFP (GC/mL; Addgene), AAV1-Ef1a-DIO-EGFP (GC/mL; Addgene), AAV2-hSyn-Cre::EGFP (GC/mL; Addgene), AAV2-hSyn-EGFP (GC/mL; Addgene), AAV1-Ef1a-DIO-GCaMP7s (GC/mL; Addgene), AAV1-CAG-DIO-$GRAB^{VIP1.0}$ (8.12 X 10^{12} GC/mL).

The mice (8–10 weeks old) selected for the experiments were anesthetized with a mixture of ketamine (100 mg/kg) and xylazine (10 mg/kg) in 0.9% saline and placed in a stereotaxic frame (RWD Life Science) for viral injection. After disinfection and craniotomy above the target region, the virus was injected using a nanoliter injector system (World Precision Instruments) at an injection rate of <100 nL/min. The coordinate for each brain regions are as follows: For SCN, AP: -1.0 mm, ML: ±0.25 mm, DV: -5.75 mm; For 20°angled injection of SCN, AP: -1.0 mm, ML: ±2.25 mm, DV: -5.5 mm; For the nucleus reuniens (RE), AP: -1.35 mm, ML: ±0.25 mm, DV: -4.6 mm ; For 20°angled injection of RE, AP: -1.0 mm, ML: ±1.62 mm, DV: -4.65 mm; For 20°angled injection of PVN, AP: -1.3, ML: ±1.96 mm, DV: -4.75 mm; For 20°angled injection of MPOA, AP: -0.45 mm, ML: ±2.09 mm, DV: -4.55 mm; For PVT, AP: -0.9 mm, ML: ±0.25 mm, DV: -3.3 mm; For lateral ventricle (LV), AP: -0.5 mm, ML: -1.0 mm, DV: -1.4 mm; For 20°angled injection of mPFC, AP: +1.7 mm, ML: ±1.3 mm, DV: -1.0 mm. Optic fibers (400 um for single fiber implantation and 200 um for bilateral, angled fiber implantation; 0.5 NA; Neurophotometrics) were placed ~100 um above viral injection coordinates. Cannula (outer diameter, 0.48 mm; inner diameter 0.34 mm; #62003, RWD Life Science) was implanted in LV for pharmacological experiments.

Intracerebroventricular (I.C.V.) Injection

VIP receptor (VIPR) antagonist ([D-p-Cl-Phe^{6},Leu^{17}]-VIP; #3054, Tocris), VIPR1 selective antagonist (PG 97-269; Bachem), and VIPR2 selective antagonist (PG 99-465; Bachem) were

prepared in artificial cerebrospinal fluid (aCSF; #35-252, Tocris) in 1 mM concentration. 2 ul of antagonists were infused into the LV at the speed of 1 ul/min. After I.C.V. injection, mice were returned to the home cage for 30 minutes before the experiment.

Virginal cytology for estrus cycle

Before the start of the experiment, estrous cycle of each female mouse was confirmed via virginal cytology. Briefly, 200-300 ul of 0.9% saline was aspirated with a disposable pipette and the virginal area was rinsed approximately 10 times. 0.9% saline containing cells from the virginal epithelium was examined under the microscope and the estrous phase of each animal was confirmed via visual inspection of the morphology of epithelial cells and neutrophils. Samples containing neutrophils (metestrus or diestrus) were excluded from the experiment, and female mice with nucleated or anuclear epithelial cells (proestrus or estrus) were used for the further experiment.

Behavioral Assays

Three-Chamber Assays: Sociability

Three-chamber apparatus was prepared with doors closed and empty wire cups placed on either side. The subject mouse was placed in the center chamber of the three-chamber apparatus and allowed habituation to the experimental setting for 5 minutes (center habituation). After center habituation, side doors were removed for free access to either chamber for 5 minutes (three-chamber habituation). After three-chamber habituation, doors were placed again with the subject mouse in the center chamber, and social and non-social cues (a male mouse and a mouse-sized object) were placed inside the wire cups on either side. After a brief time interval (2 minutes), doors were removed and the free exploration of the subject mouse between two side chambers was measured. The three-chamber apparatus was cleaned with 70% ethanol between each session.

Three-chamber Assays: Social novelty preference

After the completion of sociability measurement, doors were placed again with the subject mouse in the center chamber, and non-social cue was removed, and another social cue (a male mouse) was placed inside the wire cup. After a brief time interval (2 minutes), doors were removed and the free exploration of the subject mouse between familiar social cue and novel social cue was measured. For social novelty preference test for the female subject mice, two female mice were used as the target cue.

Three-chamber Assays: Sexual preference

After the completion of center habituation and three-chamber habituation, male and female social cue (a male and a female mice) were placed inside the wire cups on either side. After a brief time interval (2 minutes), doors were removed and the free exploration of the subject mouse between two side chambers was measured.

Three-chamber Assays: Social prioritization

After the completion of center habituation and three-chamber habituation, social and non-social cues (a female mouse and a mouse-sized object) were placed inside the wire cups on either side. After a brief time interval (2 minutes), doors were removed and the subject mouse was allowed to freely explore between two chambers (familiarization). After the completion of familiarization phase, doors were placed again with the subject mouse in the center chamber, and non-social cue was removed, and another social cue (a male mouse) was placed inside the wire

cup. After a brief time interval (2 minutes), doors were removed and the free exploration of the subject mouse between novel male cue and familiar female cue was measured (prioritization). For social prioritization test for the female subjective mice,

Three-mouse interaction (TMI) Assays

TMI assay was conducted in a square arena with sufficient bedding. Target male and female mice were labeled with a marker pen on their tail to distinguish each animal during subsequent video analysis. The subject mouse was placed inside the arena and allowed free exploration for 5 minutes (habituation). After, a female mouse was introduced into the arena for 2 minutes for direct interaction between the subject and the target mouse. After the end of 2-minute interaction, another male mouse was introduced into the arena and the free interaction between three mice was recorded for 60 minutes. The interaction time between each animal was measured for the first 5 minutes of three-mouse recording, and reproductive behavior of both the subject and the target mouse was measured for 60 minutes.

Behavior analysis

Each behavior was recorded via a camera connected to EthoVision (Noldus) software. For the three-chamber assays, the duration of each animal around the wire cups (sniffing zone) were measured and the investigation index was calculated as: ($\textit{sniffing zone duration}^{target\ 1} - \textit{sniffing zone duration}^{target\ 2}$) / ($\textit{sniffing zone duration}^{target\ 1} + \textit{sniffing zone duration}^{target\ 2}$) X 100. For quantification of the investigatory behavior during TMI assay, 5-minutes recordings of each group were manually examined and corrected using EthoVision software. The interaction time was calculated by thresholding the distance between body parts of each animal within 7 cm as 'interaction'. For quantification of reproductive behavior during TMI assay, the mounting attempt (trying to climb over the back of the female mouse with hind legs repeatedly kicking off the ground) was manually measured and mounting bout with thrusting behavior was labeled mounting success. For experiment with repeated measure between circadian time points, transition index was calculated as a subtraction of the investigation index between those time points.

Optogenetic manipulation

Mice were acclimated to the handling, patch cord attachment and three-chamber exploration (30 minutes) with the patch cord attachment 1-2 days before the experiment. For optogenetic inhibition, continuous laser with 589-nm wavelength (MSL-FN-589; CNI laser) was applied with 10-20 mW intensity at the tip of the optic cannula. The same laser intensity was kept for both 200- and 400-um optic cannula. For optogenetic activation, laser with 470-nm wavelength (MBL-FN-473; CNI laser) was applied at 10 mW intensity and 30 Hz frequency with 15 ms pulse width. Both optogenetic inhibition and activation were applied only during familiarization and prioritization sessions of social prioritization.

Fiber photometry

Calcium activity recording

Mice were acclimated to the handling, patch cord attachment and three-chamber exploration (30 minutes) with the patch cord attachment 1-2 days before the experiment. The intensity of 465-nm LED was kept around 20-30 uW at the tip of the optic cannula. Recording was conducted during social prioritization assay, with the start of each session in the assay was time-stamped using transistor-transistor logic (TTL) output signal from the EthoVision software.

VIPR activity recording

Mice were acclimated to the handling and patch cord attachment 1-2 days before the experiment. On the day of recording, the subject mouse was attached to the path cord with 465-nm LED at 10-20 uW and placed into a square arena with free access to food and water and sufficient bedding. The fluorescence was measured continuously throughout 24 hours.

Data analysis

The fiber photometry data was processed as previously described (*32*). Briefly, 465 nm (F465) and 405 nm (F405) LEDs were used for calcium-dependent and -independent excitation of GCaMP7s fluorescence, and the emitted signal was passed through a low-pass filter and demodulated using Synapse software (Tucker-Davis Technologies (TDT)). The F405 signal was used to correct motion artifacts and was normalized using the formula dF/F = (F465 – fitted F405)/fitted F405. To compare calcium response between experimental animals, global Fz was calculated as Fz = (dF/F – median(dF/F))/std(dF/F).

For peri-event histogram (PETH) analysis for each social cue, the dF/F signal was sliced and aligned to the onset of events. The signal before the event onset was used as the baseline (FB) for z-normalization. Fz was calculated as Fz = (dF/F – mean(FB))/std(FB). To quantify the global calcium level, the mean and standard deviation of the entire session were used for the calculation: Fz = (dF/F – mean(dF/F))/std(dF/F). For VIPR activity analysis, dF/F of $GRAB^{VIP1.0}$ activity was calculated in the same method with GCaMP7s recording.

Electrophysiological recordings

Slice preparation

Acute slices were prepared from VIPR2-IRES Cre mice. Transcardial perfusion was performed after anesthetizing the mice with sodium pentobarbital at 70 mg/kg. The brains were rapidly removed and immersed in chilled cutting solution of the following composition (in mM): 110 choline chloride, 2.5 KCl, 25 $NaHCO_3$, 1.25 NaH_2PO_4, 25 glucose, 0.5 $CaCl_2$, 7 $MgCl_2 \cdot 6H_2O$, 11.6 sodium L-ascorbate, and 3 pyruvic acid. Thereafter, 300 μm-thick coronal slices were prepared using a vibratome (VT1200S, Leica, Wetzlar, Germany). The slices were then incubated for 30 min at 32 °C in artificial cerebrospinal fluid (ACSF) containing the following (in mM): 119 NaCl, 2.5 KCl, 26 $NaHCO_3$, 1.25 NaH_2PO_4, 20 glucose, 2 $CaCl_2$, 1 $MgSO_4$, 0.4 L-Ascorbic acid, and 2 pyruvic acid. During sectioning, the solutions were saturated with carbogen (95% O_2, 5% CO_2) to a final pH of 7.4.

Electrophysiological recordings

The slices were transferred to a submerged recording chamber with a continuous flow of ACSF saturated with carbogen (95% O2, 5% CO2) for whole-cell patch-clamp recordings. RE $VIPR2^+$ neurons were visualized using an upright microscope (BX51WI, Olympus) equipped with differential interference contrast optics (DIC) with a 40x water immersion objective (NA 0.8, Olympus). All electrophysiological recordings were performed at 30 ± 2 °C, and fresh aCSF was perfused at approximately 1.5 mL/min. The patch electrodes were pulled from borosilicate glass capillaries to obtain a resistance between 4 and 5 MΩ. The internal solution contained the following (in mM): 138 potassium gluconate, 10 KCl, 10 HEPES, 10 Na_2-phosphocreatine, 4 MgATP, 0.3 NaGTP, and 0.2 EGTA (pH 7.25).

Drug Application

VIP (1 μM; Tocris Bioscience, Bristol, UK; Cat. No. 1911), mixed with Alexa 594 for visualization, was dissolved in artificial cerebrospinal fluid (aCSF) and loaded into a glass pipette (tip diameter: 1–2 μm). To avoid mechanical displacement of the tissue by pressure, the pipette tip was positioned slightly away from the recorded cell. Puff application was delivered using pressure pulses (30 kPa) lasting from 100 to 5000 ms.

Confocal imaging and analysis

Mice were perfused and fixed in 1X PBS and 4 % PFA after blood collection. Brains were isolated and post-fixed in 4 % PFA at 4 °C overnight. Following post-fixation for 24 hours, brains were either incubated in 30% sucrose and then frozen in an OCT compound or in PBS. Brains were sectioned at a thickness of 50 μm using a cryostat or vibratome, and every sixth section was used for subsequent analysis. The sections were stained with DAPI (1:1,000) before mounting on a glass cover. Images were obtained using a Nikon C2+ confocal microscope.

Statistics

Statistical analyses were performed using Prism (GraphPad), MATLAB (MathWorks), and R software (version 4.2.3). One-way ANOVA was used to compare multiple groups, followed by the Bonferroni post hoc test. Within-between Two-way ANOVA was used for repeated experiment in optogenetic manipulation, followed by the Bonferroni post hoc test. Paired t-test was used to compare transition index in optogenetic manipulation experiment and average VIPR activity between circadian time points. Fisher's exact test was used to compare mounting attempt percentage between groups.

Acknowledgments:

Author contributions: Conceptualization: JK, KK, HKC, Methodology: JK, JY, IP, CS, YL, JCR, HKC, Investigation: JK, JY, BK, MK, IP, JL Visualization: JK, JY, HKC, Funding acquisition: HKC, Project administration: JK, HKC, Supervision: KK, JCR, HKC, Writing – original draft: JK, HKC, Writing – review & editing: JK, HKC

Competing interests: Authors declare that they have no competing interests.

Data and materials availability: All data are available in the main text or the supplementary materials.

Fig. 1. SCN^{VIP} projection to RE is required for circadian rhythm in social priority. (**A**) Experimental scheme of social priority assay. (**B**) Representative heatmap visualization of subject mice during social priority assay in each time point. (**C** to **E**) Quantification of investigation index (C), total interaction (D), and total distance moved (E) during social priority assay in each time point. (**F** to **G**) Schematics for viral delivery (F) and an example image showing viral expression and optic fiber placement (G). (**H**) Experimental scheme of social priority assay with optogenetic inhibition. (**I**) Representative heatmap visualization of subject mice during social priority assay with optogenetic inhibition in each time point. (**J** to **M**) Quantification of investigation index (J), transition index (K), total interaction (L), and total distance moved (M) during social priority assay with or without optogenetic inhibition. (**N**-**O**) Schematics for viral delivery (N) and an example image showing viral expression and optic fiber placement (O). (**P**) Experimental scheme of social priority assay with optogenetic inhibition. (**Q**) Representative heatmap visualization of subject mice during social priority assay with optogenetic inhibition in each time point. (**R** to **U**) Quantification of investigation index (R), transition index (S), total interaction (T), and total distance moved (U) during social priority assay with or without optogenetic inhibition. n = 7, 8, 21, 13 for CT00, 06, 12, 18 groups in (C to E); n = 10 for SCN^{VIP}-eNpHR3.0 animals and n = 9 for SCN^{AVP}-eNpHR3.0 animals in (J to M); n = 8 for SCN^{VIP}-MPOA-eNpHR3.0, n = 9 for SCN^{VIP}-PVT-eNpHR3.0, n = 8 for SCN^{VIP}-PVH-eNpHR3.0, and n = 11 for SCN^{VIP}-RE-eNpHR3.0 animals (R to U). For (C to E), One-way ANOVA test followed by Tukey's HSD test; for (J), (L), (M), (R), (T), and (U), RM Two-way ANOVA test followed by pairwise paired t-test or non-parametric Two-way ANOVA test followed by Wilcoxon Signed-Rank test; for (K) and (S), paired t-test was performed. Each dot represents an individual animal. Each line represents a repeated experiment within individual animal. Data are presented as mean ± SEM. ***$P < 0.001$; **$P < 0.01$; *$P < 0.05$.

Fig. 2. RE^{VIPR2} neuron mediates circadian rhythm in social priority. (**A** to **B**) Schematics for cannula implantation (A) and an example image showing cannula placement (B). (**C**) Experimental scheme of social priority assay with systematic infusion of various pharmacological agents for VIP signaling. (**D**) Representative heatmap visualization of subject mice during social priority assay with pharmacological inhibition. (**E** to **H**) Quantification of investigation index (E), transition index (F), total interaction (G), and total distance moved (H) during social priority assay with pharmacological inhibition. (**I** to **J**) Schematics for viral delivery (I) and an example image showing viral expression (J). (**K**) Experimental scheme of social priority assay with or without genetic ablation of Vipr2 in RE. (**L**) Representative heatmap visualization of subject mice during social priority assay with or without genetic ablation of Vipr2 in RE. (**M** to **P**) Quantification of investigation index (M), transition index (N), total interaction (O), and total distance moved (P) during social priority assay with or without genetic ablation of Vipr2 in RE. n = 11, 9, 9, 10 for aCSF, VIPR, VIPR1, and VIPR2 antagonist treatment groups in (E to H). For (E), (G), (H), (M), (O), and (P), Two-way mixed ANOVA test followed by pairwise paired t-test and pairwise independent-sample t-test or non-parametric Two-way mixed ANOVA test followed by pairwise Wilcoxon Signed-Rank test and pairwise Wilcoxon Rank-Sum test; for (F), One-way ANOVA test followed by Tukey's HSD test; for (N), unpaired t-test was performed. Each dot represents an individual animal. Each line represents a repeated experiment within individual animal. Data are presented as mean ± SEM. ***$P < 0.001$; **$P < 0.01$; *$P < 0.05$.

Fig. 3. Circadian time-dependent fluctuation of VIPR signaling in RE^{VIPR2} neuron. (**A** to **B**) Schematics for viral delivery (A) and an example image showing viral expression and optic fiber

placement (B). (**C**) Experimental scheme of VIPR activity recording in freely moving animals. (**D** to **E**) Heatmap visualization of VIPR activity (D) and quantification of normalized VIPR activity (E) across two circadian timepoints. (**F**) Schematics for viral delivery and acute slice section for electrophysiological recording. (G) An example image showing Vipr2-expressing neuron with puff pipette. (H) Representative voltage-clamp trace showing a depolarizing response evoked by VIP agonist puff. Black bar indicates the timing of puff application. (I) Heatmap visualization of firing rates computed in cells that exhibited spontaneous EPSPs. Firing rate was calculated using a 500-ms sliding window. Top: aCSF puff (control); Bottom: VIP agonist puff. (J) The average Vm during the 2-second baseline period (Before), compared to the peak depolarization following the drug infusion. For (E), unpaired t-test; for (J), paired t-test was performed. Data are presented as mean ± SEM. $^{**}P < 0.01$.

Fig. 4. RE^{VIPR2} neuron and its projection to mPFC control circadian rhythm in social priority. (**A** to **B**) Schematics for viral delivery (A) and an example image showing viral expression and optic fiber placement (B). (**C**) Experimental scheme of social priority assay with optogenetic inhibition. (**D**) Representative heatmap visualization of subject mice during social priority assay with optogenetic inhibition in each time point. (**E** to **H**) Quantification of investigation index (E), transition index (F), total interaction (G), and total distance moved (H) during social priority assay with or without optogenetic inhibition. (**I** to **J**) Schematics for viral delivery (I) and an example image showing viral expression and optic fiber placement (J). (**K**) Experimental scheme of social priority assay with optogenetic inhibition. (**L**) Representative heatmap visualization of subject mice during social priority assay with optogenetic inhibition in each time point. (**M** to **P**) Quantification of investigation index (M), transition index (N), total interaction (O), and total distance moved (P) during social priority assay with or without optogenetic inhibition. n = 9 for RE^{VIPR2}-eNpHR3.0 animals and n = 8 for RE^{VIPR2}-ChR2 animals in (E to H). n = for RE^{VIPR2}-mPFC-eNpHR3.0 animals. For (E), (G), and (H), RM Two-way ANOVA test followed by pairwise paired t-test or non-parametric Two-way ANOVA test followed by Wilcoxon Signed-Rank test; for (F), paired t-test was performed. Each line represents a repeated experiment within individual animal. Data are presented as mean ± SEM. $^{***}P < 0.001$; $^{**}P < 0.01$; $^{*}P < 0.05$.

Fig. 5. Functional expression of Vipr2 in RE is essential for time-dependent naturalistic group interaction and reproductive behavior. (**A**) Schematics for viral delivery. (**B**) Experimental scheme of TMI assay (left) and illustration of group dynamics in TMI assay (right). (**C** to **E**) Quantification of investigation index (C), total interaction (D), and total distance moved (E) during TMI assay with or without genetic ablation of Vipr2 in RE. (**F**) Rastor plot of subject animals illustrating distribution of mounting attempts during TMI assay. (**G**) Latency to first mounting attempts in each time point with or without genetic ablation of Vipr2 in RE. (**H**) Cumulative plot for the proportion of animals displaying mounting attempts in each time bin. For (C to E) and (G), One-way ANOVA test followed by Tukey's HSD test; for (H), Fisher's exact test was performed. Each dot represents an individual animal. Data are presented as mean ± SEM. $^{***}P < 0.001$; $^{**}P < 0.01$; $^{*}P < 0.05$.

References and Notes

1. H. Li, Z. Zhao, S. Jiang, H. Wu, Brain circuits that regulate social behavior. *Mol. Psychiatry* **30**, 3240–3256 (2025).

2. P. Chen, W. Hong, Neural Circuit Mechanisms of Social Behavior. *Neuron* **98**, 16–30 (2018).

3. D. Wei, V. Talwar, D. Lin, Neural circuits of social behaviors: innate yet flexible. *Neuron*, doi: 10.1016/j.neuron.2021.02.012 (2021).

4. C. J. Burnett, S. C. Funderburk, J. Navarrete, A. Sabol, J. Liang-Guallpa, T. M. Desrochers, M. J. Krashes, Need-based prioritization of behavior. *eLife* **8**, e44527 (2019).

5. R. E. Brown, D. J. McFarland, Interaction of hunger and sexual motivation in the male rat: A time-sharing approach. *Anim. Behav.* **27**, 887–896 (1979).

6. A. Petzold, H. E. van den Munkhof, R. Figge-Schlensok, T. Korotkova, Complementary lateral hypothalamic populations resist hunger pressure to balance nutritional and social needs. *Cell Metab.* **35**, 456-471.e6 (2023).

7. W. H. Walker, J. C. Walton, A. C. DeVries, R. J. Nelson, Circadian rhythm disruption and mental health. *Transl. Psychiatry* **10**, 28 (2020).

8. D. Ono, D. R. Weaver, M. H. Hastings, K.-I. Honma, S. Honma, R. Silver, The Suprachiasmatic Nucleus at 50: Looking Back, Then Looking Forward. *J. Biol. Rhythm.*, 7487304231225706 (2024).

9. M. H. Hastings, E. S. Maywood, J. S. O'Neill, Cellular Circadian Pacemaking and the Role of Cytosolic Rhythms. *Curr. Biol.* **18**, R805–R815 (2008).

10. A. P. Patton, M. D. Edwards, N. J. Smyllie, R. Hamnett, J. E. Chesham, M. Brancaccio, E. S. Maywood, M. H. Hastings, The VIP-VPAC2 neuropeptidergic axis is a cellular pacemaking hub of the suprachiasmatic nucleus circadian circuit. *Nat. Commun.* **11**, 3394 (2020).

11. A. J. Harmar, H. M. Marston, S. Shen, C. Spratt, K. M. West, W. J. Sheward, C. F. Morrison, J. R. Dorin, H. D. Piggins, J.-C. Reubi, J. S. Kelly, E. S. Maywood, M. H. Hastings, The VPAC2 Receptor Is Essential for Circadian Function in the Mouse Suprachiasmatic Nuclei. *Cell* **109**, 497–508 (2002).

12. W. D. Todd, H. Fenselau, J. L. Wang, R. Zhang, N. L. Machado, A. Venner, R. Y. Broadhurst, S. Kaur, T. Lynagh, D. P. Olson, B. B. Lowell, P. M. Fuller, C. B. Saper, A hypothalamic circuit for the circadian control of aggression. *Nat. Neurosci.* **21**, 717–724 (2018).

13. A. Kukino, T. J. Walbeek, L. J. Sun, A. T. Watt, J. H. Park, A. S. Kauffman, M. P. Butler, Mistimed restricted feeding disrupts circadian rhythms of male mating behavior and female preovulatory LH surges in mice. *Horm. Behav.* **145**, 105242 (2022).

14. N. Sayar-Atasoy, I. Aklan, Y. Yavuz, C. Laule, H. Kim, J. Rysted, M. I. Alp, D. Davis, B. Yilmaz, D. Atasoy, AgRP neurons encode circadian feeding time. *Nat. Neurosci.* **27**, 102–115 (2024).

15. C. Gizowski, C. Zaelzer, C. W. Bourque, Clock-driven vasopressin neurotransmission mediates anticipatory thirst prior to sleep. *Nature* **537**, 685–688 (2016).

16. B. Collins, S. Pierre-Ferrer, C. Muheim, D. Lukacsovich, Y. Cai, A. Spinnler, C. G. Herrera, S. Wen, J. Winterer, M. D. C. Belle, H. D. Piggins, M. Hastings, A. Loudon, J. Yan, C. Földy, A. Adamantidis, S. A. Brown, Circadian VIPergic Neurons of the Suprachiasmatic Nuclei Sculpt the Sleep-Wake Cycle. *Neuron* **108**, 486-499.e5 (2020).

17. L. Kurt, A DYNAMIC THEORY OF PERSONALITY. *J. Nerv. Ment. Dis.* **84**, 612–613 (1936).

18. K. Blair, A. A. Marsh, J. Morton, M. Vythilingam, M. Jones, K. Mondillo, D. C. Pine, W. C. Drevets, J. R. Blair, Choosing the Lesser of Two Evils, the Better of Two Goods: Specifying the Roles of Ventromedial Prefrontal Cortex and Dorsal Anterior Cingulate in Object Choice. *J. Neurosci.* **26**, 11379–11386 (2006).

19. D. K. Welsh, J. S. Takahashi, S. A. Kay, Suprachiasmatic Nucleus: Cell Autonomy and Network Properties. *Annu. Rev. Physiol.* **72**, 551–577 (2010).

20. A. J. Harmar, J. Fahrenkrug, I. Gozes, M. Laburthe, V. May, J. R. Pisegna, D. Vaudry, H. Vaudry, J. A. Waschek, S. I. Said, Pharmacology and functions of receptors for vasoactive intestinal peptide and pituitary adenylate cyclase activating polypeptide: IUPHAR Review 1. *Br. J. Pharmacol.* **166**, 4–17 (2012).

21. S. Constantin, C. Quignon, K. Pizano, D. M. Shostak, S. Wray, Vasoactive intestinal peptide excites GnRH neurons via KCa3.1, a potential player in the slow afterhyperpolarization current. *Front. Cell. Neurosci.* **18**, 1354095 (2024).

22. T. M. Brown, A. T. Hughes, H. D. Piggins, Gastrin-Releasing Peptide Promotes Suprachiasmatic Nuclei Cellular Rhythmicity in the Absence of Vasoactive Intestinal Polypeptide-VPAC2 Receptor Signaling. *J. Neurosci.* **25**, 11155–11164 (2005).

23. H. Wang, T. Qian, Y. Zhao, Y. Zhuo, C. Wu, T. Osakada, P. Chen, Z. Chen, H. Ren, Y. Yan, L. Geng, S. Fu, L. Mei, G. Li, L. Wu, Y. Jiang, W. Qian, L. Zhang, W. Peng, M. Xu, J. Hu, M. Jiang, L. Chen, C. Tang, Y. Zhu, D. Lin, J.-N. Zhou, Y. Li, A tool kit of highly selective and sensitive genetically encoded neuropeptide sensors. *Science* **382**, eabq8173 (2023).

24. X. Yu, F. Jembere, K. Takehara-Nishiuchi, Prefrontal projections to the nucleus reuniens signal behavioral relevance of stimuli during associative learning. *Sci. Rep.* **12**, 11995 (2022).

25. J.-C. Cassel, A. P. de Vasconcelos, M. Loureiro, T. Cholvin, J. C. Dalrymple-Alford, R. P. Vertes, The reuniens and rhomboid nuclei: Neuroanatomy, electrophysiological characteristics and behavioral implications. *Prog. Neurobiol.* **111**, 34–52 (2013).

26. M. J. Boden, D. J. Kennaway, Circadian rhythms and reproduction. *Reproduction* **132**, 379–392 (2006).

27. Y. Li, H. Zhang, Y. Wang, D. Li, H. Chen, Advances in circadian clock regulation of reproduction. *Adv. Protein Chem. Struct. Biol.* **137**, 83–133 (2023).

28. C. P. Ritcher, Dependence of successful mating in rats on functioning of the 24-hour clocks of the male and female. *Commun. Behav. Biol.* **5**, 1–5 (1970).

29. T. Roenneberg, M. Merrow, The Circadian Clock and Human Health. *Curr. Biol.* **26**, R432–R443 (2016).

30. M. C. Antle, R. Silver, Behavioral Neuroscience of Motivation. *Curr. Top. Behav. Neurosci.* **27**, 137–169 (2015).

31. R. C. Challis, S. R. Kumar, K. Y. Chan, C. Challis, K. Beadle, M. J. Jang, H. M. Kim, P. S. Rajendran, J. D. Tompkins, K. Shivkumar, B. E. Deverman, V. Gradinaru, Systemic AAV vectors for widespread and targeted gene delivery in rodents. *Nat. Protoc.* **14**, 379–414 (2019).

32. S. Jang, I. Park, M. Choi, J. Kim, S. Yeo, S.-O. Huh, J.-W. Choi, C. Moon, H. K. Choe, Y. Choe, K. Kim, Impact of the circadian nuclear receptor REV-ERBα in dorsal raphe 5-HT neurons on social interaction behavior, especially social preference. *Exp. Mol. Med.* **55**, 1806–1819 (2023).

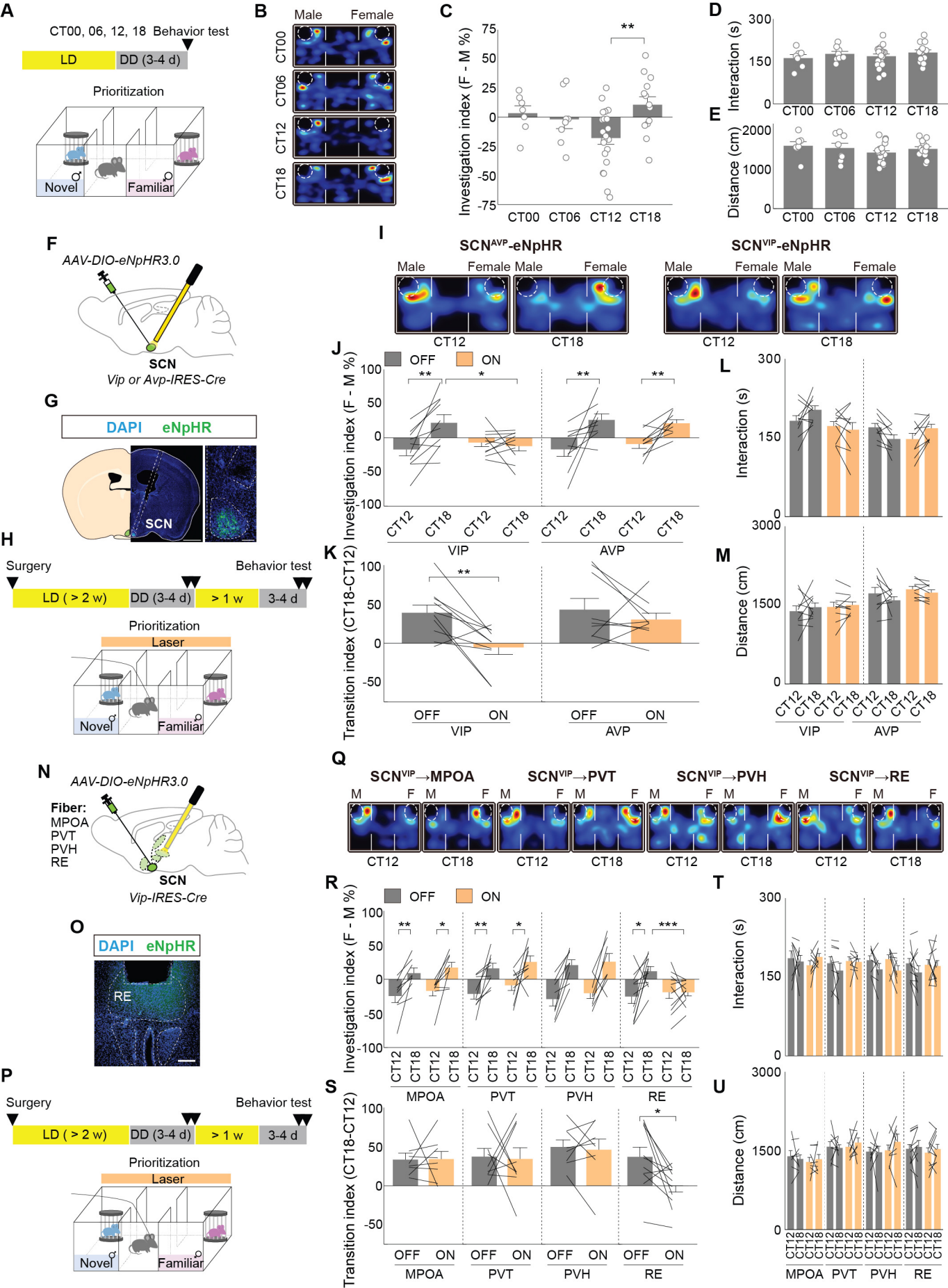
A
CT00, 06, 12, 18 Behavior test
LD
DD (3-4 d)
Prioritization
Novel
Familiar
B
Male
Female
CT00
CT06
CT12
CT18
C
Investigation index (F - M %)
CT00 CT06 CT12 CT18
D
Interaction (s)
E
Distance (cm)
F
AAV-DIO-eNpHR3.0
SCN
Vip or Avp-IRES-Cre
G
DAPI eNpHR
SCN
H
Surgery
Behavior test
LD (> 2 w)
DD (3-4 d)
> 1 w
3-4 d
Prioritization
Laser
Novel
Familiar
I
SCNAVP-eNpHR
SCNVIP-eNpHR
Male
Female
CT12
CT18
J
OFF
ON
Investigation index (F - M %)
VIP
AVP
K
Transition index (CT18-CT12)
L
Interaction (s)
M
Distance (cm)
N
AAV-DIO-eNpHR3.0
Fiber:
MPOA
PVT
PVH
RE
SCN
Vip-IRES-Cre
O
DAPI eNpHR
RE
P
Surgery
Behavior test
LD (> 2 w)
DD (3-4 d)
> 1 w
3-4 d
Prioritization
Laser
Novel
Familiar
Q
SCNVIP→MPOA
SCNVIP→PVT
SCNVIP→PVH
SCNVIP→RE
M
F
CT12
CT18
R
OFF
ON
Investigation index (F - M %)
MPOA
PVT
PVH
RE
S
Transition index (CT18-CT12)
T
Interaction (s)
U
Distance (cm)

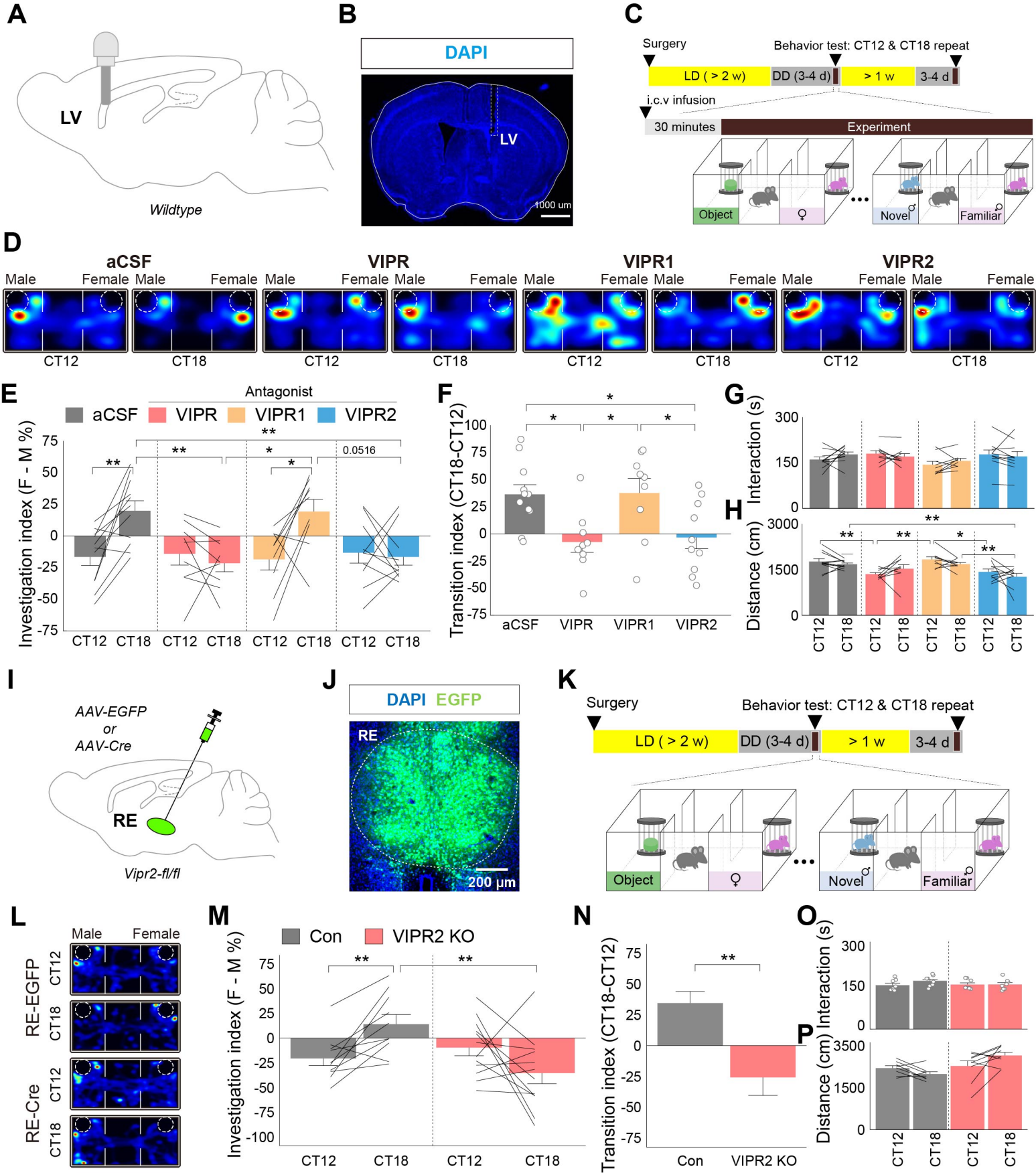
A
LV
Wildtype
B
DAPI
LV
1000 um
C
Surgery
Behavior test: CT12 & CT18 repeat
LD (> 2 w)
DD (3-4 d)
> 1 w
3-4 d
i.c.v infusion
30 minutes
Experiment
Object
Novel
Familiar
D
aCSF
VIPR
VIPR1
VIPR2
Male
Female
CT12
CT18
E
Antagonist
aCSF
VIPR
VIPR1
VIPR2
Investigation index (F - M %)
0.0516
F
Transition index (CT18-CT12)
aCSF
VIPR
VIPR1
VIPR2
G
Interaction (s)
H
Distance (cm)
I
AAV-EGFP
or
AAV-Cre
RE
Vipr2-fl/fl
J
DAPI EGFP
RE
200 µm
K
Surgery
Behavior test: CT12 & CT18 repeat
LD (> 2 w)
DD (3-4 d)
> 1 w
3-4 d
Object
Novel
Familiar
L
Male
Female
RE-EGFP
RE-Cre
CT12
CT18
M
Con
VIPR2 KO
Investigation index (F - M %)
N
Transition index (CT18-CT12)
Con
VIPR2 KO
O
Interaction (s)
P
Distance (cm)

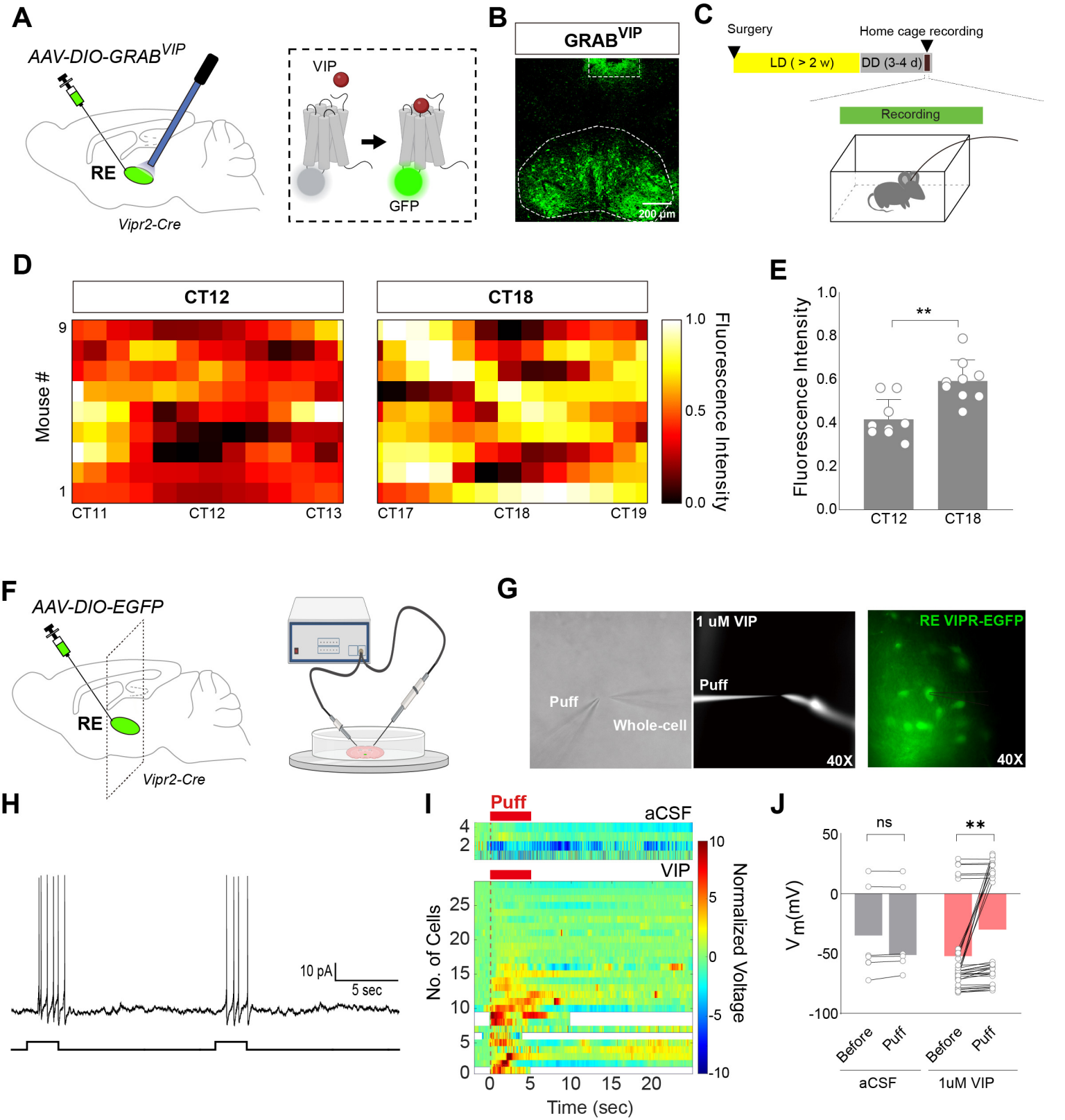
A
AAV-DIO-GRAB^VIP
RE
Vipr2-Cre
VIP
GFP
B
GRAB^VIP
200 µm
C
Surgery
Home cage recording
LD (> 2 w)
DD (3-4 d)
Recording
D
CT12
CT18
Mouse #
9
1
CT11
CT12
CT13
CT17
CT18
CT19
1.0
0.5
0.0
Fluorescence Intensity
E
Fluorescence Intensity
1.0
0.8
0.6
0.4
0.2
0.0
**
CT12
CT18
F
AAV-DIO-EGFP
RE
Vipr2-Cre
G
Puff
Whole-cell
1 uM VIP
Puff
40X
RE VIPR-EGFP
40X
H
10 pA
5 sec
I
Puff
aCSF
VIP
No. of Cells
4
2
25
20
15
10
5
0
0
5
10
15
20
Time (sec)
10
5
0
-5
-10
Normalized Voltage
J
ns
**
50
0
-50
-100
V m(mV)
Before
Puff
Before
Puff
aCSF
1uM VIP

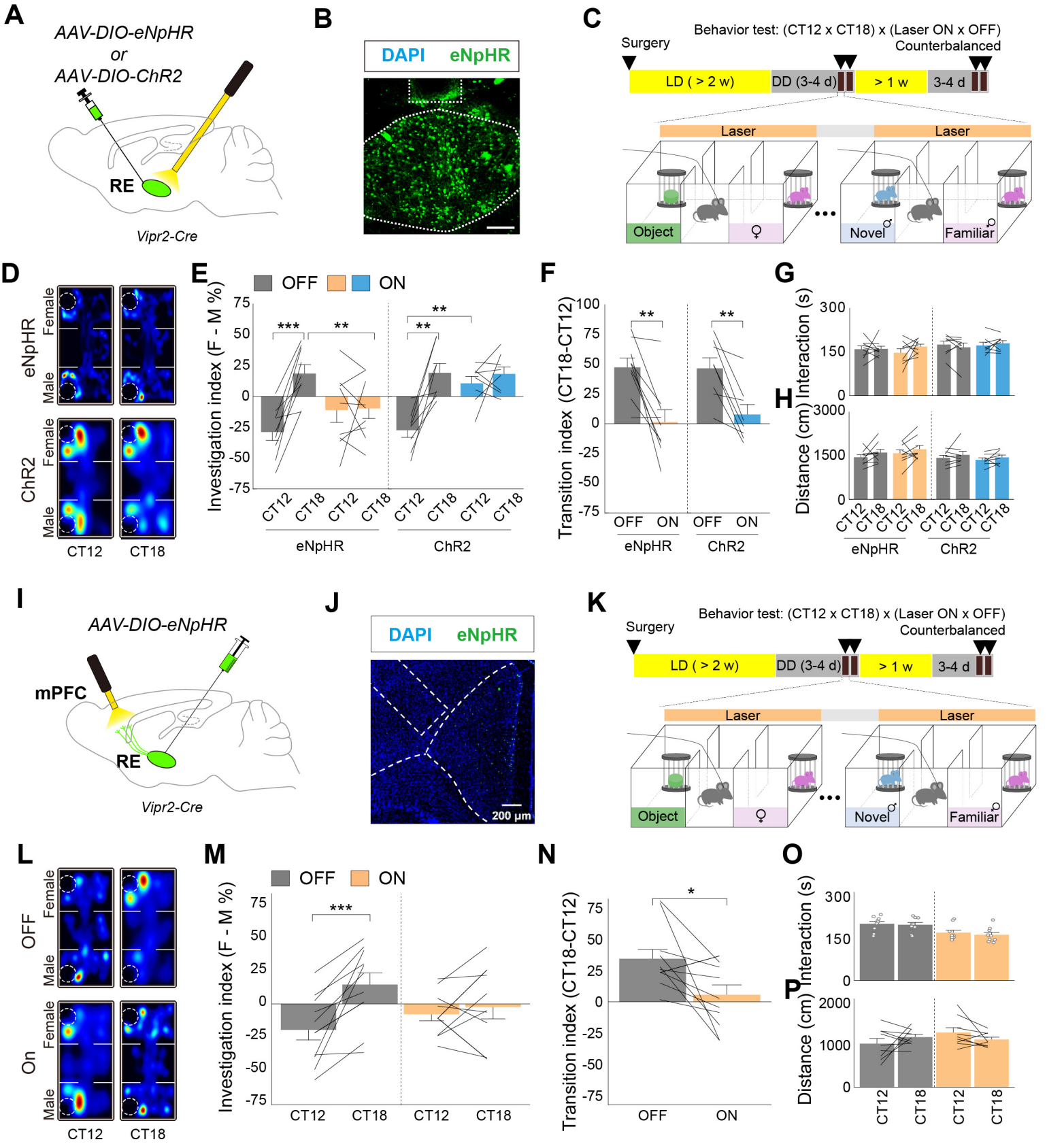
A
AAV-DIO-eNpHR
or
AAV-DIO-ChR2
RE
Vipr2-Cre
B
DAPI
eNpHR
C
Behavior test: (CT12 x CT18) x (Laser ON x OFF)
Surgery
Counterbalanced
LD (> 2 w)
DD (3-4 d)
> 1 w
3-4 d
Laser
Laser
Object
Novel
Familiar
D
eNpHR
ChR2
Female
Male
CT12
CT18
E
OFF
ON
Investigation index (F - M %)
eNpHR
ChR2
F
Transition index (CT18-CT12)
OFF
ON
G
Interaction (s)
H
Distance (cm)
I
AAV-DIO-eNpHR
mPFC
RE
Vipr2-Cre
J
DAPI
eNpHR
200 µm
K
Behavior test: (CT12 x CT18) x (Laser ON x OFF)
Surgery
Counterbalanced
LD (> 2 w)
DD (3-4 d)
> 1 w
3-4 d
Laser
Laser
Object
Novel
Familiar
L
OFF
On
Female
Male
CT12
CT18
M
OFF
ON
Investigation index (F - M %)
N
Transition index (CT18-CT12)
OFF
ON
O
Interaction (s)
P
Distance (cm)

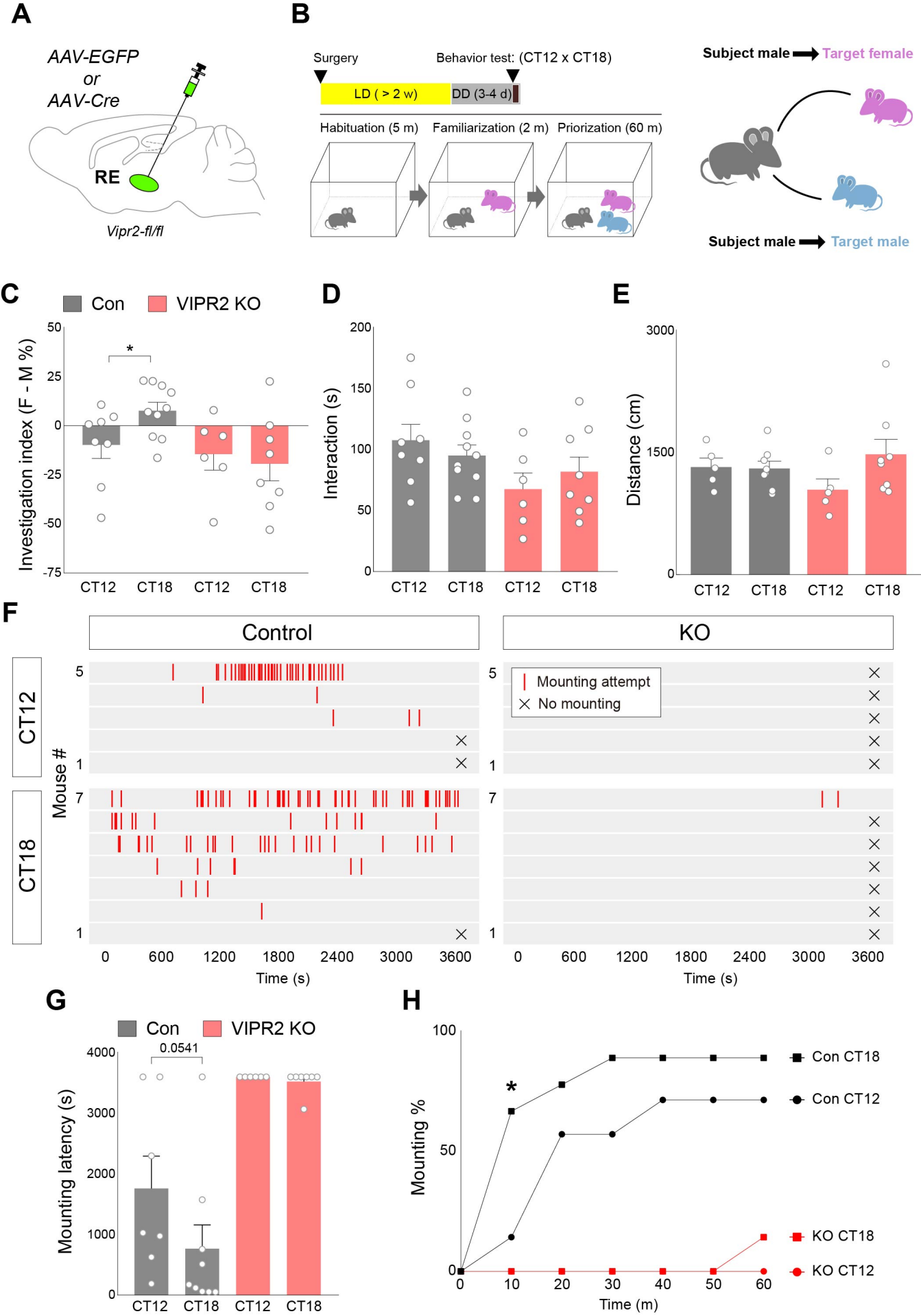
A
AAV-EGFP
or
AAV-Cre
RE
Vipr2-fl/fl
B
Surgery
Behavior test: (CT12 x CT18)
LD (> 2 w)
DD (3-4 d)
Habituation (5 m)
Familiarization (2 m)
Priorization (60 m)
Subject male
Target female
Subject male
Target male
C
Con
VIPR2 KO
Investigation index (F - M %)
50
25
0
-25
-50
-75
*
CT12
CT18
CT12
CT18
D
Interaction (s)
200
150
100
50
0
CT12
CT18
CT12
CT18
E
Distance (cm)
3000
1500
0
CT12
CT18
CT12
CT18
F
Control
KO
CT12
CT18
Mouse #
Mounting attempt
No mounting
Time (s)
0
600
1200
1800
2400
3000
3600
G
Con
VIPR2 KO
0.0541
Mounting latency (s)
4000
3000
2000
1000
0
CT12
CT18
CT12
CT18
H
Mounting %
100
50
0
*
Con CT18
Con CT12
KO CT18
KO CT12
0
10
20
30
40
50
60
Time (m)